II. Kinetic Pathways of Switching Optical Conformations in DsRed by 2D Fourier Imaging Correlation Spectroscopy

ARTICLE *in* THE JOURNAL OF PHYSICAL CHEMISTRY B · MAY 2009

Impact Factor: 3.3 · DOI: 10.1021/jp901542b · Source: PubMed

4 AUTHORS, INCLUDING:

Eric N Senning
University of Washington Seattle
21 PUBLICATIONS **103** CITATIONS
SEE PROFILE

Andrew H Marcus
University of Oregon
81 PUBLICATIONS **1,404** CITATIONS
SEE PROFILE

II. Kinetic Pathways of Switching Optical Conformations in DsRed by 2D Fourier Imaging Correlation Spectroscopy

Eric N. Senning,[†] Geoffrey A. Lott,[‡] Michael C. Fink,[§] and Andrew H. Marcus*,[†]

Departments of Chemistry and Physics, University of Oregon, Eugene, Oregon 97403, and Omega Optical, Inc., Brattleboro, Vermont 05301

Received: February 19, 2009

The kinetics of biomolecular conformational transitions can be studied by two-dimensional (2D) magnetic resonance and optical spectroscopic methods. Here we apply polarization-modulated Fourier imaging correlation spectroscopy (PM-FICS) to demonstrate a new approach to 2D optical spectroscopy. PM-FICS enables measurements of conformational fluctuations of fluorescently labeled macromolecules on a broad range of time scales ($10^{-3}-10^{2}$ s). We examine the optical switching pathways of DsRed, a tetrameric complex of fluorescent protein subunits. An analysis of PM-FICS coordinate trajectories, in terms of 2D spectra and joint probability distributions, provides detailed information about the transition pathways between distinct dipole-coupled DsRed conformations.

1. Introduction

A remarkable feature of proteins and nucleic acids is their unique ability to undergo cooperative rearrangements in structure as part of mechanisms to regulate biological activity. Rather than exist as a single, stable conformation, biological macromolecules often exhibit a broad, heterogeneous distribution of substates in thermal equilibrium.[1,2] Activation and interconversion between substates can span many decades over time.[3] Such systems exhibit complex spectra of relaxations, with principle time scales determined by transformations between substates, and exchange kinetics between different transition pathways.[4]

The kinetics of conformational transitions and chemical exchange can be studied by two-dimensional (2D) NMR spectroscopy.[4] Transitions between conformations of biological macromolecules are reflected by the magnitudes of diagonal and off-diagonal peaks in 2D NMR spectra. In recent years, chemical exchange spectroscopy has been applied at infrared and visible frequencies.[5] 2D optical methods can investigate the interconversion between populations of chemical species that are spectroscopically nonequivalent. Such 2D optical experiments measure equilibrium chemical kinetics on the time scales of the excited-state lifetimes of vibrational or electronic transitions.

In the current work, we show how polarization-modulated Fourier imaging correlation spectroscopy (PM-FICS) can probe the pathways of optical switching conformations of the fluorescent protein complex, DsRed, over a broad range of time scales much longer than the excited-state lifetime ($10^{-3}-10^{2}$ s). The PM-FICS method, and its application to DsRed, is described in the previous article (part I, DOI 10.1021/jp8093116). Similar to 2D optical and NMR methods, PM-FICS provides a phase-dependent optical signal that determines four-point time-correlation functions and the associated 2D spectra. Moreover, the information obtained from DsRed is sufficient to construct joint probability distributions of time-dependent conformational coordinates.

From a kinetic perspective, the DsRed protein is a dynamically complex heterogeneous system. Unlike monomeric variants of the green fluorescent protein (GFP),[6] DsRed is an obligate tetramer of FP subunits.[7] FPs are single chains of ~230 amino acid residues, which form an 11-stranded β-barrel with dimensions of ~3 nm × 4 nm. An α-helix inside the barrel contains the sequence of three residues that form the *p*-hydroxybenzylidene-imidazolidinone chromophore. In DsRed, the $\pi-\pi^*$ electron system of the chromophore is chemically and irreversibly extended to include an acylimine substituent, adjacent to the imidazolidinone.[8,9] This so-called maturation process occurs over the course of several days and can be followed by a gradual gain in red photoluminescence accompanied by a loss of green emission.[8,10] Nevertheless, the maturation reaction does not run to completion, even after prolonged aging, so that a given DsRed molecule likely contains at least one "immature" green chromophore.[8,11−13] The red chromophore itself undergoes switching transitions, or "flickering", between optical conformations of different emission wavelengths and intensities, and on time scales ranging between milliseconds and tens of seconds.[14−17]

Although many studies have focused on the reversible, light induced pathways between "bright" and "dark" conformations,[11,14−17] thermally driven transitions between ground states are also possible.[13,16] Detailed spectroscopic studies reveal that the red chromophore can reversibly interconvert, either through excited-state or ground-state pathways, between two brightly fluorescent red conformations (called "red" and "far-red") and a relatively dim "green" conformation.[12,13] The energetic barriers mediating these transitions are on the order of ~1000 cm^{-1} (or 12 kJ mol^{-1} $\simeq 5 \times k_B T$ at ambient temperatures). Although the physical nature of the interconversion processes remains unclear, possible mechanisms include isomerization of the protein−chromophore hydrogen-bonded network, cis−trans photoisomerization, and ground-state bond rotation.[16,18]

For our current purposes, we invoke a simplified model to interpret the conformational dynamics that influence excited-state energy transfer between adjacent chromophores in the DsRed complex. Figure 1 depicts the DsRed molecule as four cylinders (arbitrarily labeled 1−4) with principle axes oriented approximately as in the crystal structure.[7] Crystallographic data

* Corresponding Author. Phone: (541) 346-4809. Fax: (541) 346-4643. E-mail: ahmarcus@uoregon.edu.
[†] Department of Chemistry, University of Oregon.
[‡] Department of Physics, University of Oregon.
[§] Omega Optical, Inc.

10.1021/jp901542b CCC: $40.75
Published on Web 04/15/2009

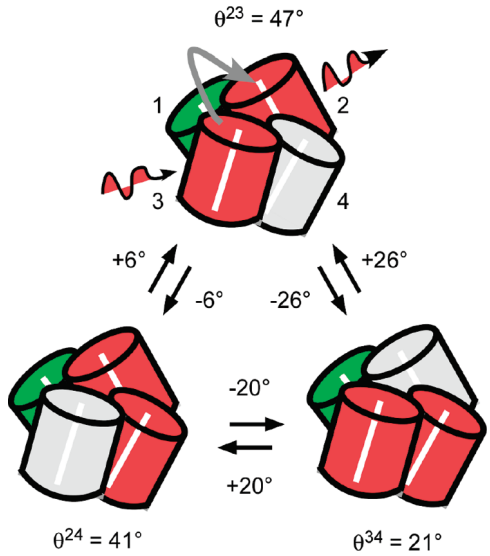

Figure 1. Optical conformational transitions of the "mature" red chromophores in DsRed. DsRed is a tetrameric complex of cylindrically shaped fluorescent protein subunits, with relative orientations approximated in the figure. Each subunit has at its center an optical chromophore that can occupy one of two chemical states, corresponding to green or red emission. The green chromophores (shaded green) do not undergo chemical conversion to the red state on the time scales of our measurements. Red chromophores can interconvert on millisecond time scales between two highly luminescent "bright" states (shaded red) and one "dark" state (shaded gray). From the crystallographic structure of DsRed, the relative angles θ^{ae} between adjacent absorption and emission transition dipole moments are known, and identified according to the numbering system shown on the top species. Polarization and spectrally selective excitation of the red chromophore subunits, mediated by electronic excitation transfer between coupled chromophores occupying adjacent sites, results in discrete transitions in the fluorescence depolarization angle $\Delta\theta^{ae}$.

suggest that there are three possible relationships between any pair of adjacent chromophores, given by the relative transition dipole orientations ($\theta^{24} = 41°$, $\theta^{23} = 47°$, and $\theta^{34} = 21°$) and the interdipole distances ($r^{24} = 43$ Å, $r^{23} = 38$ Å, and $r^{34} = 22$ Å). By symmetry, the relationships between paired transition dipoles 2−4, 2−3, and 3−4 are the same as those between 1−3, 1−4, and 1−2, respectively.[7]

As previously mentioned, most DsRed tetramers contain at least one immature green chromophore, which does not mature to red over the course of a PM-FICS measurement (~10 min). Of the sites that have matured to red (with absorption maximum $\lambda_{max} \sim 563$ nm), these undergo reversible interconversion to the far-red conformation ($\lambda_{max} \sim 577$ nm), or to the weakly fluorescent green conformation ($\lambda_{max} \sim 484$ nm), on time scales of tens of milliseconds and longer. Figure 1 depicts a DsRed molecule with a single static (immature) green site at position 1 (shaded green), and three dynamically interconverting red sites at positions 2−4. In the experiments presented below, the red optical transitions ($\lambda_{ex} \sim 532$ nm) are selectively excited, and the integrated emission from both red and far-red states is detected. Both red and far-red conformations are considered bright states (shaded red in Figure 1), while green states of the mature chromophore are dark (shaded gray). Thus, the immature green site at position 1 is pinned, while the red sites at positions 2−4 undergo reversible switching between bright and dark states. Because the distances and orientations between resonant optical transition dipoles are relatively small, an excited red chromophore can transfer its energy to one of its unexcited red or far-red neighbors by an energy transfer mechanism. When two sites in the DsRed complex are thus optically coupled, the emission polarization rotates by the angle θ^{ae}, which subtends the absorption dipole moment of the initially excited chromophore and the emission dipole moment of the emitting chromophore.[14,17] Figure 1 illustrates the three possible pairwise couplings between bright chromophore sites (for a molecule with one site pinned), and the associated depolarization angles. Also indicated are the six possible angular displacements $\Delta\theta^{ae}$ associated with conformational transitions between the three optically coupled states. Similar pairwise couplings and transitions are possible for a molecule with all of its sites red (zero sites pinned). However, for a molecule with two or more of its sites pinned, transitions between distinct pairwise coupled conformations are not possible, and such species are not expected to contribute to the fluctuating emission signals.

The model depicted in Figure 1 is consistent with available experimental data for DsRed. However, little is known about the details of such thermally activated switching transitions, such as whether they occur at random or in a cooperative manner due to interactions between adjacent FP subunits. For example, a cooperative mechanism could involve a series of optical conformations, dynamically connected along multiple kinetic pathways. The following work demonstrates how 2D PM-FICS can determine such information about the optical transitions of multicolored FPs by monitoring the coordinate fluctuations of a finite population of molecules.

2. Experimental Methods

2.1. PM-FICS Observables. The equilibrium coordinate fluctuations of a finite population of DsRed molecules in 95% glycerol/water solution were monitored by the PM-FICS method, as described in part I (DOI 10.1021/jp8093116). The measurement observables are the number density $Z^{ND}_{k_G}(t) \propto \langle \exp i[k_G x(t)] \rangle$ and the anisotropy density $Z^{AD}_{k_G}(t) \propto \langle \exp i[k_G x(t) - 2\theta^{ae}(t)] \rangle$, where the angle brackets indicate a sum over the $\sim 10^6$ molecules in the illuminated sample volume. In these expressions, $x(t)$ and $\theta^{ae}(t)$ are time-dependent position and conformation coordinates, respectively. We interpret these signals using the first-order cumulant approximation (discussed in part I, DOI 10.1021/jp8093116).

2.2. Four-Point Time-Correlation Functions. Four-point time-correlation functions (TCFs) for the number density and anisotropy density fluctuations were constructed from products of four sequential data points:

$$C^{(4)}_{ND}(t_{43}, t_{32}, t_{21}) \equiv \langle Z^{ND^*}_{k_G}(0) Z^{ND}_{k_G}(t_{21}) Z^{ND}_{k_G}(t_{32}+t_{21}) Z^{ND^*}_{k_G}(t_{43}+t_{32}+t_{21}) \rangle \quad (1)$$

and

$$C^{(4)}_{AD}(t_{43}, t_{32}, t_{21}) \equiv \langle Z^{AD^*}_{k_G}(0) Z^{AD}_{k_G}(t_{21}) Z^{AD}_{k_G}(t_{32}+t_{21}) Z^{AD^*}_{k_G}(t_{43}+t_{32}+t_{21}) \rangle \quad (2)$$

Equations 1 and 2 define the time intervals t_{43} (=$t_4 - t_3$), t_{32}, and t_{21} with $t_4 \geq t_3 \geq t_2 \geq t_1 \geq 0$. In the first-order cumulant approximation, eqs 1 and 2 can be written

$$C^{(4)}_{ND}(t_{43}, t_{32}, t_{21}) = \left\langle \exp\left[-\frac{1}{2} k_G{}^2 \delta\Delta\bar{x}_N{}^2(t_{21})\right] \right\rangle \left\langle \exp\left[-\frac{1}{2} k_G{}^2 \delta\Delta\bar{x}_N{}^2(t_{43})\right] \right\rangle \langle \exp ik_G[\Delta\bar{x}_N(t_{43}) - \Delta\bar{x}_N(t_{21})] \rangle \quad (3)$$

and

$$C^{(4)}_{AD}(t_{43}, t_{32}, t_{21}) = C^{(4)}_{ND}(t_{43}, t_{32}, t_{21}) C^{(4)}_{A}(t_{43}, t_{32}, t_{21}) \quad (4)$$

where

$$C_A^{(4)}(t_{43}, t_{32}, t_{21}) = \langle \exp[-2\delta\Delta\bar{\theta}_N^{ae2}(t_{21})]\rangle\langle \exp[-2\delta\Delta\bar{\theta}_N^{ae2}(t_{43})]\rangle\langle \exp i2[\Delta\bar{\theta}_N^{ae}(t_{43}) - \Delta\bar{\theta}_N^{ae}(t_{21})]\rangle \quad (5)$$

Equation 3 defines the time-ordered displacements of the mean center of mass, $\Delta\bar{x}_N(t_{21})$ [$=\bar{x}_N(t_2) - \bar{x}_N(t_1)$] and $\Delta\bar{x}_N(t_{43})$, which occur during successive time intervals t_{21} and t_{43}, respectively. Similarly, eq 4 defines the time-ordered displacements of the mean depolarization angle, $\Delta\bar{\theta}_N^{ae}(t_{21})$ and $\Delta\bar{\theta}_N^{ae}(t_{43})$. Equation 4 suggests that the anisotropy TCF can be determined from the ratio $C_A^{(4)}(t_{43}, t_{32}, t_{21}) = C_{AD}^{(4)}(t_{43}, t_{32}, t_{21})/C_{ND}^{(4)}(t_{43}, t_{32}, t_{21})$. These four-point TCFs have similar mathematical forms to those employed in two-dimensional optical and magnetic resonance spectroscopy.[19] Four-point TCFs contain information about correlations of events that occur during the intervals t_{43} and t_{21}, and decay on time scales for which the magnitudes of the collective phase displacements deviate by an amount $\sim\pi/4$. Such correlations diminish with increasing waiting period t_{32}, so that they appear indistinguishable from the products of functionally independent two-point TCFs. It is therefore useful to focus on the t_{32} dependence of the difference correlation functions $C^{(4)}(t_{43},t_{32},t_{21}) - C^{(2)}(t_{43})C^{(2)}(t_{21})$.

2.3. Two-Dimensional Spectral Densities. It is convenient to represent the four-point TCFs in the frequency domain, through their partial Fourier transform, with respect to t_{43} and t_{21}

$$S^{(4)}(\nu_{43}, t_{32}, \nu_{21}) = \int_0^\infty dt_{43}\int_0^\infty dt_{21}[C^{(4)}(t_{43}, t_{32}, t_{21}) - C^{(2)}(t_{43})C^{(2)}(t_{21})]e^{i\nu_{21}t_{21}+i\nu_{43}t_{43}} \quad (6)$$

The 2D spectral density is given by the absolute value $|S^{(4)}(\nu_{43}, t_{32}, \nu_{21})|$, plotted in the $\nu_{21}-\nu_{43}$ plane. The 2D spectral density is related to the joint probability that the system undergoes two successive coordinate displacements at the transition rates ν_{21} and ν_{43}, separated in time by the interval t_{32}. Such 2D spectra are similar to those obtained by magnetic resonance and optical techniques, and can provide information about the rates of chemical processes.

2.4. Two-Dimensional Distribution Functions. Information about weights and magnitudes of correlated displacements can be obtained from four-point distribution functions (DFs). We define $P^{(4)}[\Delta\bar{x}_N(t_{43}); \Delta\bar{x}_N(t_{21})]$ as the joint probability density of sequentially sampling N molecules whose mean center of mass undergoes two successive displacements, $\Delta\bar{x}_N(t_{21})$ and $\Delta\bar{x}_N(t_{43})$, during the intervals t_{21} and t_{43}, respectively. We construct the joint distributions by sampling four-point products of the form $Z_{k_G}^{ND*}(0)Z_{k_G}^{ND}(t_{21})Z_{k_G}^{ND}(t_{32} + t_{21})Z_{k_G}^{ND*}(t_{43} + t_{32} + t_{21}) = \exp[-(1/2)k_G^2\delta\Delta\bar{x}_N^2(t_{21})]\exp[-(1/2)k_G^2\delta\Delta\bar{x}_N^2(t_{43})]\exp ik_G[\Delta\bar{x}_N(t_{43}) - \Delta\bar{x}_N(t_{21})]$. Such products are used to calculate 2D histograms of the joint probability to observe mean center-of-mass displacements during consecutive time intervals. As discussed in part I (DOI 10.1021/jp8093116), if the center-of-mass displacements are uncorrelated, then the joint distribution can be factored into a product of two-point DFs, i.e., $P^{(2)}[\Delta\bar{x}_N(t_{43})]P^{(2)}[\Delta\bar{x}_N(t_{21})]$. For such Brownian systems of diffusing molecules, the joint distribution is expected to be a two-dimensional Gaussian centered about the coordinate $\Delta\bar{x}_N(t_{43}) = \Delta\bar{x}_N(t_{21}) = 0$.

2D distributions are similarly defined for displacements of the mean depolarization angle. $P^{(4)}[\Delta\bar{\theta}_N^{ae}(t_{43}); \Delta\bar{\theta}_N^{ae}(t_{21})]$ is the joint distribution associated with consecutive displacements of conformation, which is constructed from four-point products of the anisotropy density $Z_{k_G}^{AD*}(0)Z_{k_G}^{AD}(t_{21})Z_{k_G}^{AD}(t_{32} + t_{21})Z_{k_G}^{AD*}(t_{43} + t_{32} + t_{21}) = Z_{k_G}^{ND*}(0)Z_{k_G}^{ND}(t_{21})Z_{k_G}^{ND}(t_{32} + t_{21})Z_{k_G}^{ND*}(t_{43} + t_{32} + t_{21})Z^{A*}(0)Z^{A}(t_{21})Z^{A}(t_{32} + t_{21})Z^{A*}(t_{43} + t_{32} + t_{21})$. It is possible to divide the above expression by the contributions from the number density to isolate the anisotropy effects alone, i.e., $Z^{A*}(0)Z^{A}(t_{21})Z^{A}(t_{32} + t_{21})Z^{A*}(t_{43} + t_{32} + t_{21}) = \exp[-2\delta\Delta\bar{\theta}_N^{ae2}(t_{21})]\exp[-2\delta\Delta\bar{\theta}_N^{ae2}(t_{43})]\exp i2[\Delta\bar{\theta}_N^{ae}(t_{43}) - \Delta\bar{\theta}_N^{ae}(t_{21})]$. As we discuss below, such four-point DFs contain detailed information about correlated changes in the conformation of coupled dipoles of the DsRed complex.

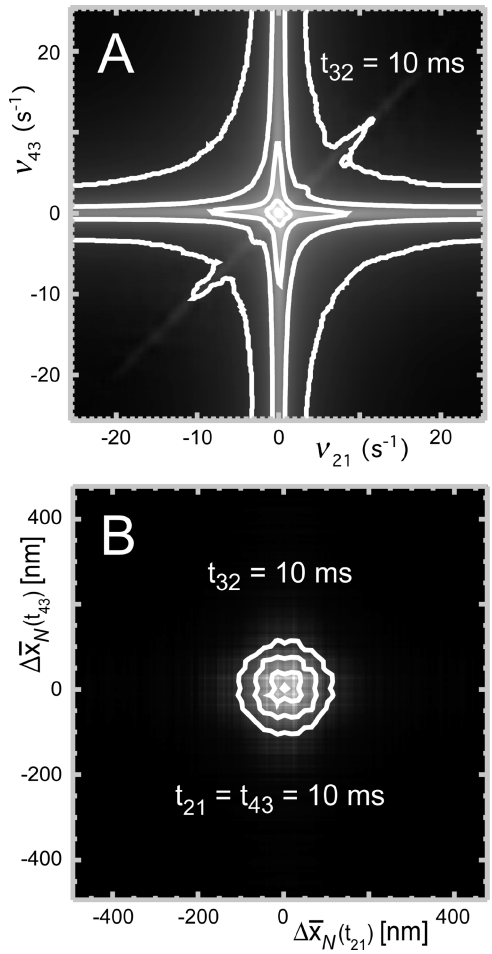

Figure 2. Contour diagrams of the two-dimensional spectral density and the joint distribution function of center-of-mass displacements. In panel A is shown the logarithm of $|S_{ND}^{(4)}(\nu_{21}, t_{32}, \nu_{43})|$ versus ν_{21} and ν_{43} for a single value of the waiting period $t_{32} = 10$ ms. The line shape is nearly Lorentzian, centered at the peak value $\nu_{21} = \nu_{43} = 0$. In panel B is shown the joint distribution $P_N^{(4)}[\Delta\bar{x}_N(t_{21}), t_{32}, \Delta\bar{x}_N(t_{43})]$ for the values $t_{21} = t_{32} = t_{43} = 10$ ms. The 2D distribution is approximately Gaussian, and centered about the origin with $\Delta\bar{x}_N(t_{21}) = \Delta\bar{x}_N(t_{43}) = 0$.

3. Results and Discussion

In Figure 2, we present results for the 2D spectral density and the joint DF of the mean center-of-mass displacements. In Figure 2A is shown the logarithm of $|S_{ND}^{(4)}(\nu_{21}, t_{32}, \nu_{43})|$ in the $\nu_{21}-\nu_{43}$ plane, for $t_{32} = 10$ ms. Because the TCFs for DsRed translational motion decay exponentially, the Fourier-transform-related spectral density (see eq 6) is Lorentzian. For $t_{32} \leq 20$ ms, a minor feature is observed along the diagonal line $\nu_{21} = \nu_{43}$, indicating correlated motion on these relatively short time scales. For $t_{32} > 20$ ms, the feature along the diagonal disappears (data not shown). In Figure 2B is shown the joint distribution $P_N^{(4)}[\Delta\bar{x}_N(t_{21}); \Delta\bar{x}_N(t_{43})]$ evaluated at $t_{21} = t_{32} = t_{43} = 10$ ms. For all values of t_{32} investigated, the joint DF appears as a two-dimensional Gaussian consistent with Brownian motion. These

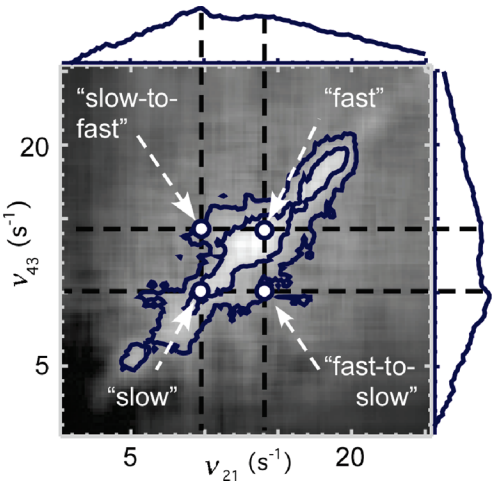

Figure 3. Logarithm of the two-dimensional spectral density of the mean depolarization angles $|S_A^{(4)}(\nu_{21}, t_{32}, \nu_{43})|$, for waiting period $t_{32} = 20$ ms. Features along the diagonal line (labeled "fast" and "slow") indicate the distribution of conformational transition rates, while off-diagonal features indicate molecular populations that "exchange" between conformational transition rates. Along the horizontal and vertical axes is projected the magnitude of the spectrum, evaluated at the diagonal $\nu_{21} = \nu_{43}$. Contours are shown at 0.5 and 0.25 times the peak height.

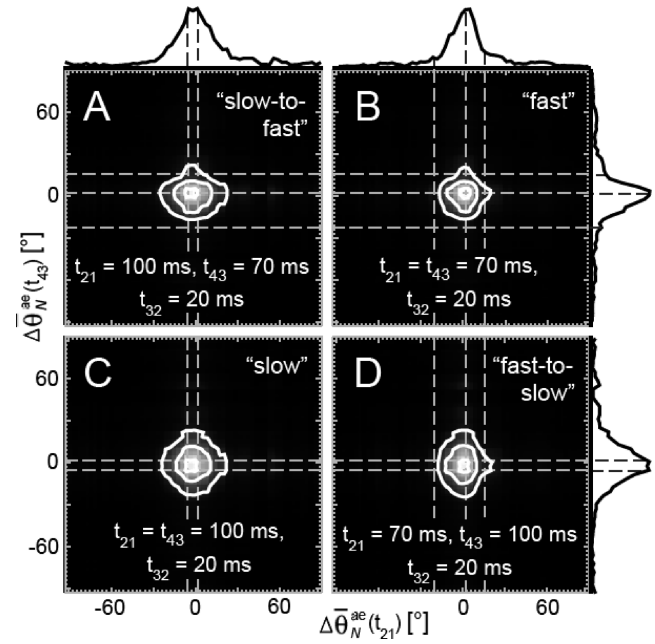

Figure 4. Joint distributions of the sampled mean displacements of depolarization angles $P^{(4)}[\Delta\bar{\theta}_N^{ae}(t_{43}); \Delta\bar{\theta}_N^{ae}(t_{21})]$, where the waiting period $t_{32} = 20$ ms, and $t_{21}, t_{43} \in \{70$ ms, 100 ms$\}$, as shown. Selected features in the joint distributions (indicated by horizontal and vertical dashed gray lines) reflect temporally correlated transitions that participate in "fast" (~70 ms) and "slow" (~100 ms) conformational transition pathways. The magnitudes of the distributions are projected onto horizontal and vertical axes. Contours are shown at 0.9, 0.5, and 0.25 times the peak height.

results support the view that cooperative center-of-mass displacements do not play a significant role in DsRed dynamics on the time scales of the current measurements.

Having established an accurate picture of the center-of-mass dynamics for DsRed, it is possible to apply the factorization procedure outlined in section 2.2 to determine the 2D spectrum of anisotropy fluctuations. In Figure 3 is shown the logarithm of the two-dimensional spectral density $|S_A^{(4)}(\nu_{21}, t_{32}, \nu_{43})|$ as a contour diagram in the $\nu_{21}-\nu_{43}$ plane, with $t_{32} = 20$ ms. Features that appear on the line diagonal to the spectrum ($\nu_{21} = \nu_{43}$) indicate sampled populations that maintain their rate of conformational transitions over the duration of the waiting period. Features that lie off the diagonal line, i.e., $\nu_{21} \neq \nu_{43}$, represent populations that undergo transitions between distinct regions of the spectrum during the waiting period. In Figure 3, the magnitude of the spectrum evaluated at the diagonal line is projected onto the horizontal and vertical axes. The sampled populations are broadly distributed among transition rates ranging from 0 to 25 Hz, and are roughly partitioned into two peaks centered at ~10 and 14 Hz. In Figure 3, these peaks are labeled "slow" and "fast", and are indicated by vertical and horizontal dashed lines. At the intersections of the dashed lines are diagonal features associated with "slow" and "fast" populations. Off-diagonal features are labeled "slow-to-fast" and "fast-to-slow," to indicate molecular subpopulations that make transitions between the two spectral regions. Because the 2D spectrum is narrow in the direction of the antidiagonal ($\nu_{21} = -\nu_{43}$), the sampled populations do not readily exchange between fast and slow spectral regions on the time scale of ~20 ms.

We next determine joint DFs that contribute to the spectral line shape. In Figure 4 are shown contour diagrams of $P^{(4)}[\Delta\bar{\theta}_N^{ae}(t_{43}); \Delta\bar{\theta}_N^{ae}(t_{21})]$ corresponding to each of the four labeled points in the 2D spectrum shown in Figure 3. Features in the joint DF can establish the existence of "pathways" between adjacent conformational transitions. For each of the DFs shown in Figure 4, the values of the intervals are $t_{32} = 20$ ms and t_{21}, $t_{43} \in \{70$ ms, 100 ms$\}$, which were chosen to correspond to the labeled points in the spectral density. Along the horizontal and vertical axes are shown the projected magnitudes, which span the range ±30°. These DFs were constructed from histograms of ~35 000 four-point products. The procedure was repeated to ensure reproducibility of independent data sets, and the results were averaged together to produce the DFs shown in Figure 4.

For the two DFs representing diagonal features of the spectral density (labeled "fast" and "slow"), both exhibit mirror plane symmetry with respect to the diagonal line $[\Delta\bar{\theta}_N^{ae}(t_{21}) \simeq \Delta\bar{\theta}_N^{ae}(t_{43})]$. For the two DFs representing off-diagonal features (labeled "slow-to-fast" and "fast-to-slow"), each exhibits the projections of the "fast" and "slow" DFs onto one another. The joint DFs exhibit numerous peaks and shoulders, which undoubtedly reflect the conformational transitions of a complex heterogeneous system. In our current analysis, we focus on a subset of these peaks (indicated by vertical and horizontal dashed lines in Figure 4). For the DF representing "slow" displacements (Figure 4C), there are peaks centered at the coordinates $[\Delta\bar{\theta}_N^{ae}(t_{21}), \Delta\bar{\theta}_N^{ae}(t_{43})] = (-6°, -6°)$, $(+2°, -6°)$, and $(-6°, +2°)$. For the distribution representing "fast" displacements (Figure 4B), there are peaks at the coordinates $(+2°, +2°)$, $(+16°, +16°)$, $(+2°, +16°)$, $(+2°, -22°)$, $(+16°, +2°)$, and $(-22°, +2°)$. These peaks indicate correlated events, in which a change in molecular conformation of a given magnitude is temporally correlated to that of another. The diagonal symmetry of the "fast" and "slow" DFs suggests that, for the relatively short waiting period of $t_{32} = 20$ ms, there is no temporal bias to indicate which of the two correlated events precedes the other.

The above results suggest that there are two significant optical conformation pathways in DsRed: (i) a "slow" pathway connecting at least two sequential steps, which involve the angular displacements $\Delta\bar{\theta}_N^{ae} = +2°$ and $-6°$ and (ii) a "fast" pathway connecting at least three sequential steps, which involve the displacements $\Delta\bar{\theta}_N^{ae} = +2°$, $+16°$, and $-22°$. As discussed above, the coordinate pairings given by the joint DFs indicate

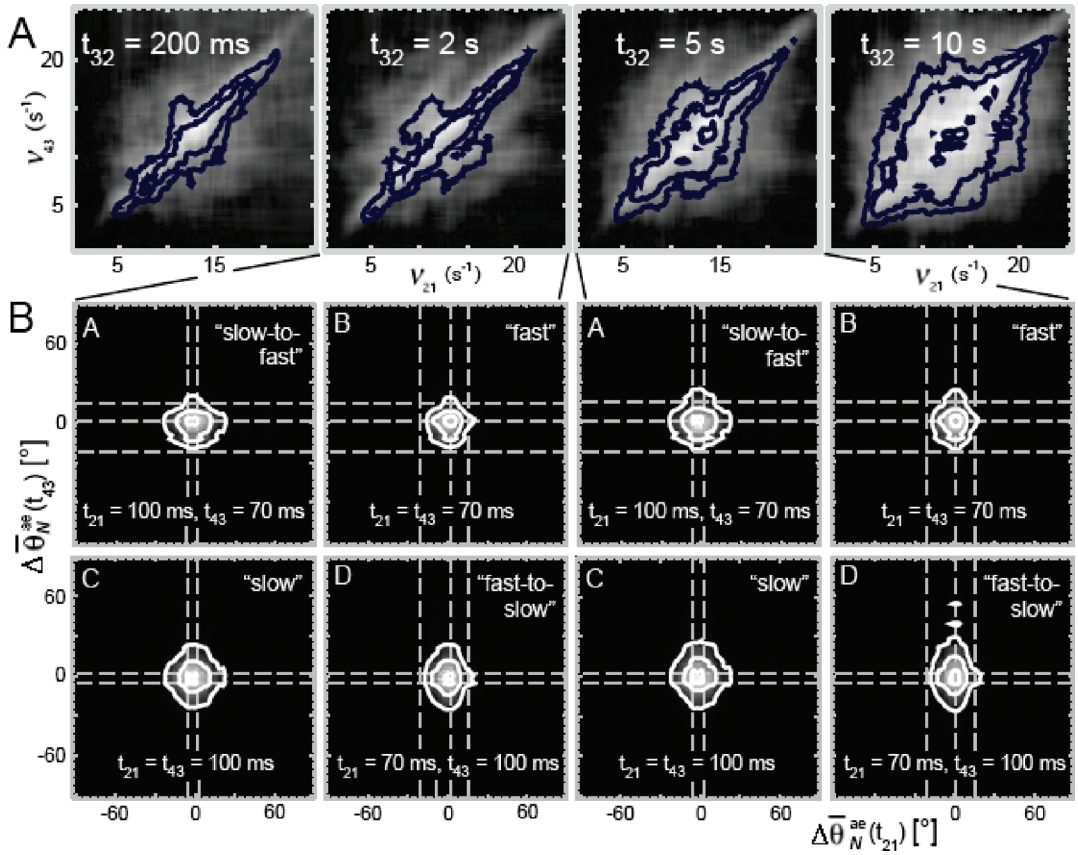

Figure 5. (A) Logarithm of the two-dimensional spectral density of the sampled mean depolarization angles $|S^{(4)}_A(\nu_{21}, t_{32}, \nu_{43})|$, for $t_{32} = 200$ ms, 2 s, 5 s, and 10 s. The transverse broadening indicates that the average exchange time scale of the anisotropy fluctuations is approximately the same as the mean relaxation time $\tau_A = 8$ s. (B) Joint distributions $P^{(4)}[\Delta\bar{\theta}^{ae}_N(t_{43}); \Delta\bar{\theta}^{ae}_N(t_{21})]$, with $t_{32} = 2$ and 5 s.

the adjacencies between sequential steps in a given pathway. For example, the "fast" pathway appears to contain adjacent conformational transitions with $\Delta\bar{\theta}^{ae}_N = -22°$ and $+2°$, since the points $(+2°, -22°)$ and $(-22°, +2°)$ are present in the joint DF shown in Figure 4B. On the other hand, the "fast" pathway does not contain adjacent transitions with $\Delta\bar{\theta}^{ae}_N = -22°$ and $+16°$, because the joint distribution has no significant magnitude at the points $(+16°, -22°)$ and $(-22°, +16°)$. The distributions representing off-diagonal features in the spectral density (Figure 4A and D) contain information about exchange processes between the fast and slow pathways. For the distribution representing "slow-to-fast" exchange (Figure 4A), features are present at the coordinates $(+2°, +2°)$, $(+2°, +16°)$, $(+2°, -22°)$, $(-6°, +2°)$, $(-6°, -22°)$, and $(-6°, +16°)$. For the distribution representing "fast-to-slow" exchange (Figure 4D), features are present at the coordinates $(+2°, +2°)$, $(+2°, -6°)$, $(+16°, +2°)$, $(+16°, -6°)$, $(-22°, +2°)$, and $(-22°, -6°)$. Features present in the exchange distributions indicate bridging steps between "fast" and "slow" kinetic pathways.

Information about the time scale for exchange between "fast" and "slow" kinetic pathways is obtained from the t_{32} dependence of the 2D spectrum. In Figure 5A is shown the logarithm of $|S^{(4)}_A(\nu_{21}, t_{32}, \nu_{43})|$ for sequentially increasing values of the waiting period: $t_{32} = 200$ ms, 2 s, 5 s, and 10 s. As the value of t_{32} is increased, the spectral density broadens in the transverse (off-diagonal) direction on the time scale of a few seconds. This transverse broadening indicates that subpopulations of molecules in the "fast" pathway undergo exchange with molecular populations in the "slow" pathway. The average time scale for the exchange is roughly the same as the $\tau_A = 8$ s relaxation time for the anisotropy two-point TCF, reported in part I (DOI 10.1021/jp8093116). Nevertheless, the behavior of the joint DFs indicates that the elementary steps of the exchange processes occur on subsecond time scales. In Figure 5B are shown two sets of the joint distributions, corresponding to $t_{32} = 2$ and 5 s. These DFs exhibit features at the same coordinates as those observed for the $t_{32} = 20$ ms DFs (indicated by dashed lines). As the waiting period is increased, there is a gradual loss of diagonal symmetry for "fast" and "slow" DFs (subpanels B and C, respectively), such that they broaden in the direction of the vertical axis. As discussed further below, this loss of diagonal symmetry corresponds to the introduction of a temporal bias that indicates which of the two correlated transitions precedes the other. Furthermore, the loss of diagonal symmetry suggests a tendency for molecular population to flow from the "fast" to "slow" pathways during the waiting period.

4. Conclusions

Millisecond conformational dynamics of freely diffusing DsRed was studied using a four-point analysis of PM-FICS trajectories. The 2D spectrum of conformational transitions, $|S^{(4)}_A(\nu_{21}, t_{32}, \nu_{43})|$, is roughly partitioned into "fast" and "slow" kinetic pathways. The slow anisotropy relaxation time $\tau_A = 8$ s is characteristic of exchange between "fast" and "slow" molecular subpopulations. Detailed information about the pathways connecting adjacent conformational transitions is contained by the joint distributions, $P^{(4)}[\Delta\bar{\theta}^{ae}_N(t_{43}); \Delta\bar{\theta}^{ae}_N(t_{21})]$. For waiting periods much shorter than the exchange time ($t_{32} \ll \tau_A$), there is a clear separation between molecular subpopulations participating in each of the two pathways. For the "fast" subpopulation, the angular displacements $\Delta\bar{\theta}^{ae} = +2°$, $+16°$, and $-22°$ are

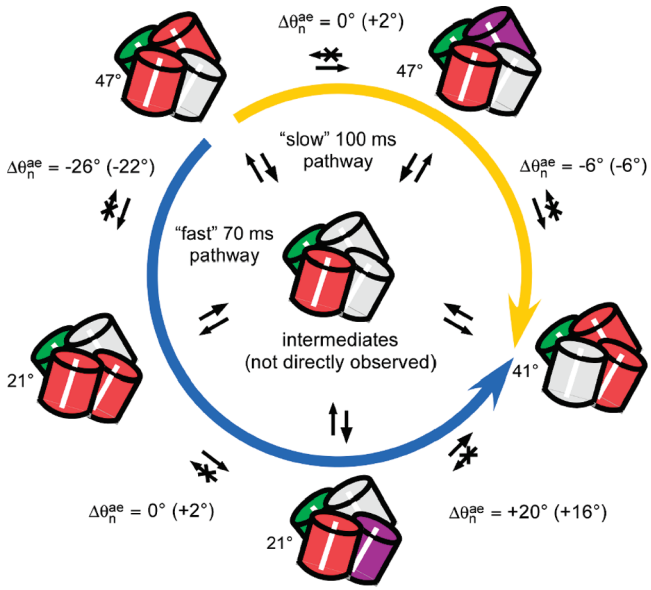

Figure 6. Possible model for the conformational transition pathways observed in DsRed. The structural and color conventions are the same as those adopted in Figure 1, except that the "far-red" chromophore state is indicated by purple shading. The measured displacements in the depolarization angle are shown in parentheses next to the expected values from the crystallographic data. The molecule undergoes temporally correlated (cooperative) transitions between different optically coupled conformations. There are distinct "fast" and "slow" transition pathways, operating on the 70 and 100 ms time scales, respectively (indicated by the blue and gold arrows). Intermediates lacking dipolar coupling, such as the one generically depicted at the center of the diagram, connect adjacent species. Exchange processes involve correlations between transitions that occur on separate pathways and occur on the mean time scale of 8 s.

observed, with adjacent pairings $+2° \leftrightarrow +16°$ and $+2° \leftrightarrow -22°$. For the "slow" subpopulation, the paired displacements $\Delta\bar{\theta}^{ae} = +2°$ and $-6°$ are observed.

Our results can be combined with the model discussed in section 1 for the possible depolarization angles of DsRed optical conformations. We propose the mechanism illustrated in Figure 6 to partially account for our observations of the conformational transition pathways. The system is assumed to be at equilibrium, with average steady-state concentrations of species maintained by balanced differential rates of interconversion. On the basis of the crystal structure of DsRed,[7] three conformations are possible for which the coupled dipoles have relative orientations $\theta_n^{ae} = 47°$, 41°, and 21° (see Figure 1). Spectral shifts at individual chromophore sites result in conformational transitions. The "fast" pathway, indicated by the blue arrow, consists of three temporally correlated steps: $-22° \rightarrow +2° \rightarrow +16°$. The "slow" pathway, indicated by the gold arrow, consists of two temporally correlated steps: $+2° \rightarrow -6°$. For each step is indicated the observed (in parentheses) and the expected angular displacements accompanying the conversion between species. In both transition pathways, observations of the angular displacement $\Delta\bar{\theta}^{ae} = +2°$ are assigned to conformational transitions in which a red site is converted into a far-red site (purple). The similarities between optical properties of the red and far-red states likely correspond to a very small change in the transition dipole moment orientation. It is also hypothesized that intermediates lacking dipolar coupling, such as the one generically depicted at the center of the diagram, connect adjacent species. While there is a directional bias implied by the proposed mechanism, the time ordering of events is interchangeable. A conformational transition upstream in the pathway is correlated to an adjacent downstream transition. Nevertheless, for $t_{32} \ll \tau_A$, the time ordering of events is not established. That is, an upstream transition is as likely to occur before a downstream transition as it is likely to occur after one. Features in the exchange distributions indicate correlations between transitions on separate pathways. Therefore, molecules participating in one reactive pathway can participate in the other pathway at a later time. For $t_{32} \ll \tau_A$, the exchange processes are symmetric; for each exchange process involving transfer of molecular population from the "fast" to the "slow" pathway, there is an equally weighted exchange process in the opposite direction.

As the waiting period is increased to values exceeding the mean relaxation time, the loss of diagonal symmetry of the "fast" and "slow" joint distributions $P^{(4)}[\Delta\bar{\theta}_N^{ae}(t_{43}); \Delta\bar{\theta}_N^{ae}(t_{21})]$ (see Figure 5B) indicates the introduction of temporal bias. For $t_{32} \geq \tau_A$, downstream transitions tend to occur with greater probability after the waiting period. Corresponding inverse processes, in which downstream events occur prior to upstream events, receive less weight. Furthermore, the broadening of the exchange distributions occurs in an asymmetric manner. While the "fast-to-slow" distribution appears to elongate in the direction of the $\Delta\bar{\theta}_N^{ae}(t_{43})$ axis, the "slow-to-fast" distribution does so to a lesser extent. This indicates that exchange processes between "fast" and "slow" pathways are more heavily biased in the "fast-to-slow" direction.

In this work, we have demonstrated a new 2D optical approach to study the kinetics of equilibrium conformational transitions of biological macromolecules, over a wide range of time scales (10^{-3}–10^2 s). Polarization-modulated Fourier imaging correlation spectroscopy (PM-FICS) was applied to simultaneously monitor molecular center-of-mass and anisotropy fluctuations. When applied to the system of DsRed molecules undergoing free diffusion, the approach allowed us to isolate the effects of optical switching conformational transitions. The phase selectivity of PM-FICS measurements enables the calculation of 2D distributions and spectral densities. Similar to established 2D spectroscopic methods, the 2D spectral density determined by PM-FICS is useful to decompose the kinetics of a dynamically heterogeneous system, such as DsRed, into its separate components. A unique feature of PM-FICS is its ability to determine joint probability distributions of coordinate displacements, which contain detailed information about the pathways connecting sequential conformational transitions.

The PM-FICS method shares common attributes with 2D optical spectroscopy, single-molecule spectroscopy, and fluorescence fluctuation spectroscopy. The detailed information provided by PM-FICS measurements should be useful to address broad ranging problems in the fields of protein and nucleic acid dynamics, as well as other areas in complex systems. In the current work, the well-defined structure of the DsRed molecule made this an appealing candidate to demonstrate the potential of the approach. The ability to perform such measurements on proteins and nucleic acids of general interest, in solution and in cell compartments, could enable future studies of *in vivo* enzymatic function.

Acknowledgment. We thank Prof. Jeffrey Cina for useful discussions. We acknowledge support for this research from the National Institutes of Health R01 GM67891 and the National Science Foundation CHE-0303715.

References and Notes

(1) Frauenfelder, H.; Wolynes, S. G.; Sligar, P. G. The energy landscapes and motions of proteins. *Science* **1991**, *254*, 1598–1603.

(2) Miyashita, O.; Onuchic, J. N.; Wolynes, P. G. Nonlinear elasticity, proteinquakes, and the energy landscapes of functional transitions in proteins. *Proc. Natl. Acad. Sci. U.S.A.* **2003**, *100*, 12570–12575.

(3) Henzler-Wildman, K. A.; Lei, M.; Thai, V.; Kerns, S. J.; Karplus, M.; Kern, D. A heirarchy of timescales in protein dynamics is linked to enzyme catalysis. *Nature (London)* **2007**, *450*, 913–918.

(4) Boehr, D. B.; Dyson, H. J.; Wright, P. E. An NMR perspective on enzyme dynamics. *Chem. Rev.* **2006**, *106*, 3055–3079.

(5) Hochstrasser, R. M. Two-dimensional spectroscopy at the infrared and optical frequencies. *Proc. Natl. Acad. Sci. U.S.A.* **2007**, *104*, 14190–14196.

(6) Shaner, N. C.; Campbell, R. E.; Steinbach, P. A.; Giepmans, B. N. G.; Palmer, A. E.; Tsien, R. Y. Improved monomeric red, orange, and yellow fluorescent proteins derived from Discosoma sp. red fluorescent protein. *Nat. Biotechnol.* **2004**, *22*, 1567–1572.

(7) Wall, M. A.; Socolich, M.; Ranaganathan, R. The structural basis for red fluorescence in the tetrameric GFP homolog DsRed. *Nat. Struct. Biol.* **2000**, *7*, 1133–1138.

(8) Gross, L. A.; Baird, G. S; Hoffman, R. C; Baldridge, K. K.; Tsien, R. Y. The structure of the chromophore within DsRed, a red fluorescent protein from coral. *Proc. Natl. Acad. Sci. U.S.A.* **2000**, *97*, 11990–11995.

(9) Yarbrough, D.; Wachter, R. M.; Kallio, K.; Matz, M. V.; Remington, S. J. Refined crystal structure of DsRed, a red fluorescent protein from coral, at 2.0-A resolution. *Proc. Natl. Acad. Sci. U.S.A.* **2001**, *98*, 462–467.

(10) Baird, G. S.; Zacharias, D. A.; Tsien, R. Y. Biochemistry, mutagenesis, and oligomerization of DsRed, a red fluorescent protein from coral. *Proc. Natl. Acad. Sci. U.S.A.* **2000**, *97*, 11984–11989.

(11) Garcia-Parajo, M. F.; Koopman, M.; van Dijk, E. M. H. P.; Subramaniam, V.; van Hulst, N. F. The nature of fluorescence emission in the red fluorescent protein DsRed, revealed by single-molecule detection. *Proc. Natl. Acad. Sci. U.S.A.* **2001**, *98*, 14392–14397.

(12) Bonsma, S.; Gallus, J.; Konz, F.; Purchase, R.; Volker, S. Light-induced conformational changes and energy transfer in red fluorescent protein. *J. Lumin.* **2004**, *107*, 203–212.

(13) Bonsma, S.; Purchase, R.; Jezowski, S.; Gallus, J.; Konz, F.; Volker, S. Green and red fluorescnt proteins: photo- and thermally induced dynamics probed by site-selective spectroscopy and hole burning. *ChemPhysChem* **2005**, *6*, 838–849.

(14) Heikal, A. A.; Hess, S. T.; Baird, G. S.; Tsien, R. Y.; Webb, W. W. Molecular spectroscopy and dynamics of intrinsically fluorescent proteins: coral red (dsRed) and yellow (Citrine). *Proc. Natl. Acad. Sci. U.S.A.* **2000**, *97*, 11996–12001.

(15) Malvezzi-Campeggi, F.; Jahnz, M.; Heinze, K. G.; Dittrich, P.; Schwille, P. Light-induced flickering of DsRed provides evidence for distinct and interconvertible fluorescence states. *Biophys. J.* **2001**, *81*, 1776–1785.

(16) Schenk, A.; Ivanchenko, S.; Rocker, C.; Wiedenmann, J.; Nienhaus, G. U. Photodynamics of red fluorescent proteins studied by fluorescence correlation spectroscopy. *Biophys. J.* **2004**, *86*, 384–394.

(17) Lounis, B. J.; Deich, F. I.; Rosell, S. G.; Boxer, W. E. Moerner, Photophysics of DsRed, a red fluorescent protein, from the ensemble to the single-molecule level. *J. Phys. Chem. B* **2001**, *105*, 5048–5054.

(18) Hendrix, J.; Flors, C.; Dedecker, P.; Hofkens, J.; Engelborghs, Y. Dark states in moneric red fluorescent proteins studied by fluorescence correlation and single molecule spectroscopy. *Biophys. J.* **2008**, *94*, 4103–4113.

(19) Mukamel, S. *Principles of Nonlinear Optical Spectroscopy*; Oxford University Press: Oxford, U.K., 1995.

JP901542B